Molecular mechanism for depolarization-induced modulation of Kv channel closure

Alain J. Labro,[1,2] Jerome J. Lacroix,[1] Carlos A. Villalba-Galea,[3] Dirk J. Snyders,[2] and Francisco Bezanilla[1]

[1]Department of Biochemistry and Molecular Biology, University of Chicago, Chicago, IL 60637
[2]Department of Biomedical Sciences, University of Antwerp, Antwerp 2610, Belgium
[3]Department of Physiology and Biophysics, Virginia Commonwealth University School of Medicine, Richmond, VA 23298

Voltage-dependent potassium (Kv) channels provide the repolarizing power that shapes the action potential duration and helps control the firing frequency of neurons. The K^+ permeation through the channel pore is controlled by an intracellularly located bundle-crossing (BC) gate that communicates with the voltage-sensing domains (VSDs). During prolonged membrane depolarizations, most Kv channels display C-type inactivation that halts K^+ conduction through constriction of the K^+ selectivity filter. Besides triggering C-type inactivation, we show that in *Shaker* and Kv1.2 channels (expressed in *Xenopus laevis* oocytes), prolonged membrane depolarizations also slow down the kinetics of VSD deactivation and BC gate closure during the subsequent membrane repolarization. Measurements of deactivating gating currents (reporting VSD movement) and ionic currents (BC gate status) showed that the kinetics of both slowed down in two distinct phases with increasing duration of the depolarizing prepulse. The biphasic slowing in VSD deactivation and BC gate closure was strongly correlated in time and magnitude. Simultaneous recordings of ionic currents and fluorescence from a probe tracking VSD movement in *Shaker* directly demonstrated that both processes were synchronized. Whereas the first slowing originates from a stabilization imposed by BC gate opening, the subsequent slowing reflects the rearrangement of the VSD toward its relaxed state (relaxation). The VSD relaxation was observed in the *Ciona intestinalis* voltage-sensitive phosphatase and in its isolated VSD. Collectively, our results show that the VSD relaxation is not kinetically related to C-type inactivation and is an intrinsic property of the VSD. We propose VSD relaxation as a general mechanism for depolarization-induced slowing of BC gate closure that may enable Kv1.2 channels to modulate the firing frequency of neurons based on the depolarization history.

INTRODUCTION

Voltage-gated potassium (Kv) channels form transmembrane potassium-selective pathways that actively open and close in response to changes in membrane potential. In vivo, these channels are (commonly) responsible for repolarizing the membrane potential back to its resting conditions after an action potential (Hodgkin and Huxley, 1952). The kinetics and abundance of these channels shape the action potential and constitute a critical determining factor of cellular excitability. A typical Kv channel is composed of four individual α subunits (MacKinnon, 1991), each containing six membrane-spanning helices (S1–S6) whereby S5 and S6 segments organize to form a central ion-conducting pore (Doyle et al., 1998; Long et al., 2005). This K^+ permeation pathway can be sealed off by two separate gates in series: (1) at the level of the K^+ selectivity filter that collapses and becomes nonpermeable upon C-type inactivation (Liu et al., 1996; Loots and Isacoff, 1998) and (2) at the inner S6 bundle-crossing (BC) gate, which closes or opens depending on the membrane potential (Liu et al., 1997; del Camino and Yellen, 2001).

Control over the BC gate is achieved by the four voltage-sensing domains (VSDs) formed by the S1 through S4 segments that surround the central pore domain. The S4 segment, which contains positively charged amino acids (gating charges), forms the main voltage-sensing element that switches between resting and active conformations upon changes in the membrane potential. This motion is mechanically transmitted via the S4–S5 linker ($S4S5_L$) to the BC gate of the same subunit (Labro et al., 2005; Long et al., 2005), thereby closing or opening the channel's pore. The dynamics of the VSD motion can be directly monitored by measuring transient gating currents that are produced by the displacement of the gating charges across the membrane electric field (Bezanilla, 2000).

A.J. Labro and J.J. Lacroix contributed equally to this paper.
Correspondence to Francisco Bezanilla: fbezanilla@uchicago.edu

Abbreviations used in this paper: BC, bundle crossing; Ci-VSP, *Ciona intestinalis* voltage-sensitive phosphatase; MES, methylsulfonate; TMRM, tetramethyl-rhodamine-5-maleimide; VSD, voltage-sensing domain; WT, wild type.

The Rockefeller University Press $30.00
J. Gen. Physiol. Vol. 140 No. 5 481–493
www.jgp.org/cgi/doi/10.1085/jgp.201210817

In addition to its resting and active states, the VSD also enters a relaxed state upon prolonged depolarizations (Villalba-Galea et al., 2008). In *Shaker* K^+ channels, relaxed VSDs return to their resting state twice as slow as from their active state, thus resulting in an apparent shift of the charge (Q) vs. voltage (V [QV]) curves toward negative voltages (Lacroix et al., 2011). Using in-depth biophysical analysis of wild-type (WT) *Shaker* and Kv1.2 channels, we report here that prolonged depolarizations also produce a twofold slowing down of BC gate closure with a time course synchronized with VSD relaxation. Upon prolonged depolarizations, K^+ permeation is in several Kv channels terminated via a constriction of the selectivity filter known as C-type inactivation (Loots and Isacoff, 1998; Cuello et al., 2010). As part of these experiments were done in the KcsA channel that lacks a VSD, these results strongly convey the notion that C-type inactivation does not require the presence of a VSD. In agreement with this notion, we provide here compelling evidence that VSD relaxation occurs independently from C-type inactivation and propose that VSD relaxation constitutes a potent physiological molecular mechanism for the modulation of deactivating ionic currents in Kv channels.

MATERIALS AND METHODS

Expression in *Xenopus laevis* oocytes

The *Shaker* cDNA used in this study was the fast inactivation removed (IR, Δ6–46) version described previously (Yellen et al., 1991), and the WT human Kv1.2 and *Ciona intestinalis* voltage-sensitive phosphatase (Ci-VSP) cDNAs were kindly provided by S. Goldstein (Brandeis University, Boston, MA) and Y. Okamura (Osaka University, Osaka, Japan), respectively. cDNAs were cloned into a pBSTA vector modified for enhanced expression into *Xenopus* oocytes (Starace and Bezanilla, 2001). The Ci-VSP cDNA contained the C363S mutation that inactivates catalytic activity (Murata et al., 2005). cDNAs were linearized with a unique NotI restriction site (New England Biolabs, Inc.) and transcribed into cRNAs using a T7 RNA expression kit (Ambion; Invitrogen). 5–50 ng cRNA was injected into mature *Xenopus* oocytes 4–24 h after surgical extraction from adult frogs. Injected oocytes were maintained before recordings in a standard oocyte solution containing 100 mM NaCl, 5 mM KCl, 2 mM $CaCl_2$, and 10 mM HEPES, pH 7.5, supplemented with 50 µg/ml gentamycin for 2–6 d at 16.5°C.

Electrophysiology and solutions

Ionic and gating current recordings were taken at room temperature with a high performance oocyte clamp amplifier (CA-1B; Dagan Corporation) in the cut-open voltage-clamp setup. Current recordings were digitized with an in-house–built acquisition system based on the a4d4 module in a digital signal processing unit (SB6711; Innovative Integration) at a sampling frequency ranging from 10 to 100 kHz after 5–20-kHz low-pass filtering. Pulse protocols and data acquisition were controlled using in-house–developed software. Recording pipettes with a resistance of 0.8–1.5 MΩ were pulled from 1.5-mm borosilicate glass capillaries (World Precision Instruments) using a vertical heat filament micropipette puller (P87; Sutter Instrument). For gating current recordings, remaining capacitive transient currents after compensation were subtracted online using the −P/4 method for activation protocols (−120-mV holding potential) and +P/4 for deactivation protocols (20-mV holding potential) when possible. For ionic current recordings, the external solution contained 11.5 mM K-methylsulfonate (MES), 103.5 mM NMDG-MES, 2 mM Ca-MES, and 10 mM HEPES, and the internal solution contained 115 mM K-MES, 2 mM EGTA, and 10 mM HEPES, both adjusted to pH 7.5 using MES. Gating currents were recorded after depleting the oocytes of K^+ by repetitive activation of the channels. Any remaining ionic current contamination was eliminated by external TEA block, and the external recording solution contained 115 mM TEA-MES, 2 mM Ca-MES, and 10 mM HEPES adjusted to pH 7.5 using MES. The internal solution contained 115 mM NMDG-MES, 2 mM EGTA, and 10 mM HEPES adjusted to pH 7.5.

Site-directed fluorimetry

To study VSD movement using site-directed voltage-clamp fluorimetry, we chose the M356C *Shaker* mutant because labeling this residue has been shown to give nice time-dependent changes in fluorescence amplitude (ΔF) that follow VSD movements (Cha and Bezanilla, 1997). Oocytes expressing the *Shaker* mutant M356C were incubated in 0.2 mM dithiothreitol for 30 min before labeling with 20 µM tetramethyl-rhodamine-5-maleimide (TMRM; Invitrogen) for 20 min on ice. Labeled cells were individually mounted on an epifluorescence cut-open oocyte setup and illuminated with a tungsten halogen lamp as previously described (Cha and Bezanilla, 1997). TMRM fluorescence was measured using an excitation filter (535DF35), a 570-nm dichroic mirror, and an emission filter (595AF60; Omega Filters).

Data analysis

Details of pulse protocols used to elicit gating or ionic currents were adjusted to determine the biophysical properties of each construct adequately and are shown in the figures or described in legends. The obtained charge versus voltage (QV) and conductance versus voltage (GV) curves were fitted with the following Boltzmann equation: $y = 1/\{1 + \exp[-(V - V_{1/2})/k]\}$, where V represents the applied voltage, $V_{1/2}$ is the midpoint potential at which 50% of the total charge has moved or half of the channels have opened, and k is the slope factor. The time constants of the activating and deactivating gating currents (I_{gON} and I_{gOFF}) were determined by fitting the decaying part of the current traces with a single or double exponential function. The kinetics of the ionic currents were determined by fitting the rise in current activation (I_{ac}) or decay during deactivation (I_{deac}) with a single or double exponential function, respectively. When a double exponential fit was used, a weighted mean time constant was calculated based on the contribution (amplitude) of each component.

Signals for simultaneous ionic currents and fluorescence recordings were not subtracted and analogically filtered at 5–10 kHz. Fluorescence traces were further digitally filtered at 1–5 kHz. The procedure for fitting the fluorescence changes induced by the pulses was similar to that described in the previous paragraph. All results are expressed as means ± SEM, with n being the number of oocytes analyzed.

RESULTS

Strong correlation between VSD movement and BC gate opening/closure in *Shaker* channels

To investigate the coupling between the VSD and the BC gate during channel opening and closure, we first recorded ionic currents (reporting on the BC gate status) in *Shaker* channels expressed in *Xenopus* oocytes. Next, gating currents (reporting VSD movement) were

recorded from the same cells by replacing internal and external K^+ ions by the nonpermeant cation NMDG (Fig. 1, A and B). The voltage dependence of BC gate opening/closure, shown by the GV curve, displayed a half-activation voltage ($V_{1/2}$) of −30.0 ± 2.1 mV and a slope of 8.3 ± 0.7 mV (n = 8; Fig. 1 C). We determined the amount of gating charge displaced by the VSD for each voltage pulse by integrating gating currents over the pulse duration. When the gating currents were generated by pulsing from a constant hyperpolarized initial voltage to incremental depolarized voltages (activation protocol; Fig. 1 B), the integration of the gating currents produced during the depolarizing test pulses (Ig_{ON}) or repolarizing postpulses (Ig_{OFF}) yielded a similar QV curve with a $V_{1/2}$ of −47.5 ± 1.1 mV and a slope of 8.0 ± 0.9 mV (n = 6; Fig. 1 C). To obtain the voltage dependence of VSD deactivation, gating currents were generated by pulsing from a constant depolarized voltage to more negative voltages (deactivation protocol; Fig. 1 D). Integration of the Ig_{OFF} gating currents produced during the repolarizing test pulses resulted in a QV curve with a $V_{1/2}$ of −63.7 ± 1.2 mV and a slope of 9.9 ± 1.0 mV (n = 5; Fig. 1 C). A similar approximately −15-mV difference in the $V_{1/2}$ values of the QV curves between the voltage dependence of activation and deactivation has been ascribed to either an intrinsic difference of voltage sensitivity of the VSD between its resting or active position or to an undetected slow gating component in Ig_{OFF} (Lacroix et al., 2011).

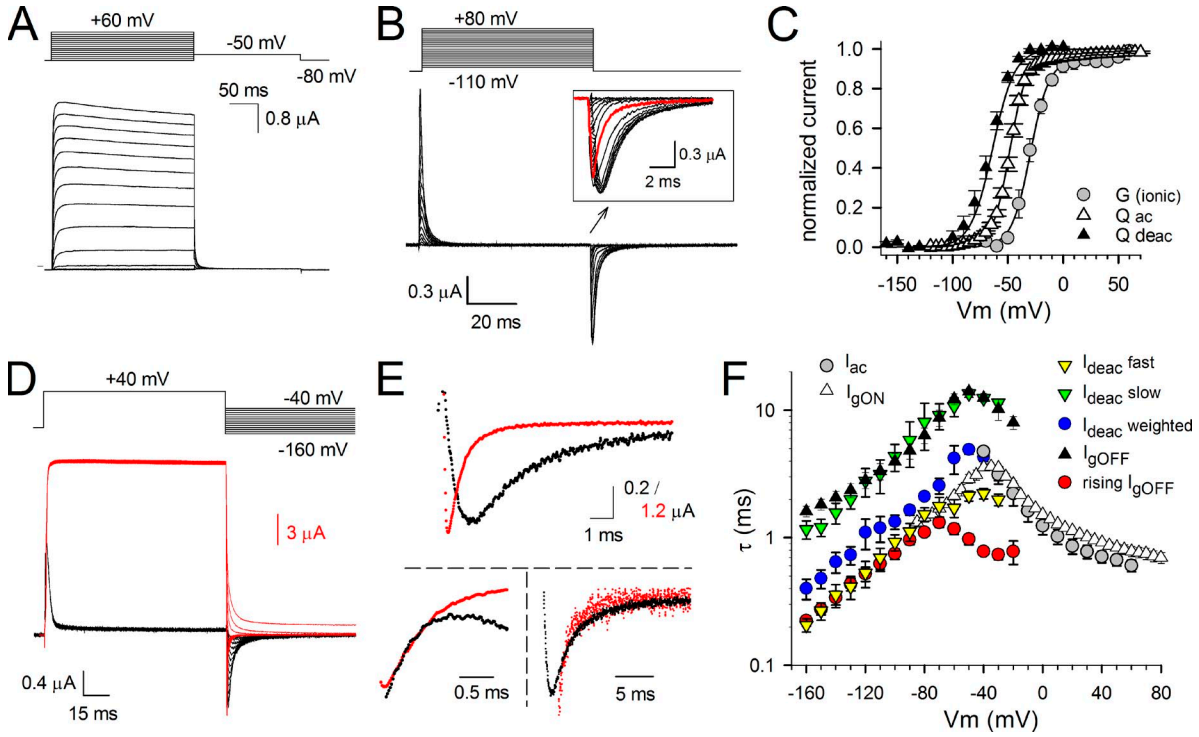

Figure 1. Ionic and gating currents from *Shaker*-H4-IR; behavior of the VSD and channel gate. (A) Activating ionic currents (I_{ac}) recorded from *Shaker*-H4-IR using the pulse protocol shown on top. (B) Gating current recordings after depletion of K^+ and external TEA block. The holding potential was −130 mV, and oocytes were depolarized in 5-mV increments from −120 to 80 mV. Background leak and capacitive currents were subtracted with a −P/4 protocol using a −120-mV holding potential. The inset is a scaled-up view of the I_{gOFF} currents highlighting the gradual slowing in I_{gOFF} decay when prepulse depolarization voltages became stronger (red trace is I_{gOFF} for a −50-mV pulse). (C) Voltage dependence of both activating and deactivating charge movement (QV curve) and BC gate opening (GV curve). The GV curve (circles) was obtained from the ionic tail currents during the repolarization step of pulse protocols shown in A. The voltage dependence of gating charge activation (QV curve displayed with open triangles; Q_{ac}) was obtained by integrating the repolarizing gating currents (I_{gOFF}) of the activation protocol shown in B. The voltage dependence of gating charge deactivation was obtained by integrating the repolarizing gating currents of the deactivation protocol shown in D (QV curve displayed with closed triangles; Q_{deac}). Both GV and QV values were normalized, and the curves shown are for both GV and QV the average fit to a Boltzmann equation. (D) Superposition of scaled ionic (red traces) and gating currents (black traces) obtained from the same oocyte using the voltage protocol shown on top. Scale bars for gating and ionic currents are shown in black and red, respectively. (E, top) A scaled-up view of the overlapping deactivation ionic (I_{deac}) and gating (I_{gOFF}) currents from D at −110-mV repolarizing voltage. (bottom) The respective I_{deac} and I_{gOFF} currents were normalized and superimposed. On the left, the I_{gOFF} is inverted to highlight the overlap of the fast component in I_{deac} with the rising phase observed in I_{gOFF}. On the right, a scaled-up view of the slow component in I_{deac} that matches the I_{gOFF} decay. (F) Voltage dependency of the time constants ± SEM of I_{gON} decay (open triangles; n = 8), I_{gOFF} decay (closed triangles; n = 7), the rising phase of I_{gOFF} (red circles; n = 7), I_{ac} (gray circles; n = 7), the fast component of I_{deac} (yellow inverted triangles; n = 7), the slow component of I_{deac} (green inverted triangles; n = 7), and the weighted I_{deac} kinetics (blue circles; n = 7). Note the superposition of the slow I_{deac} component with I_{gOFF} decay and the fast I_{deac} component with the rising phase in I_{gOFF}. Error bars represent SEM.

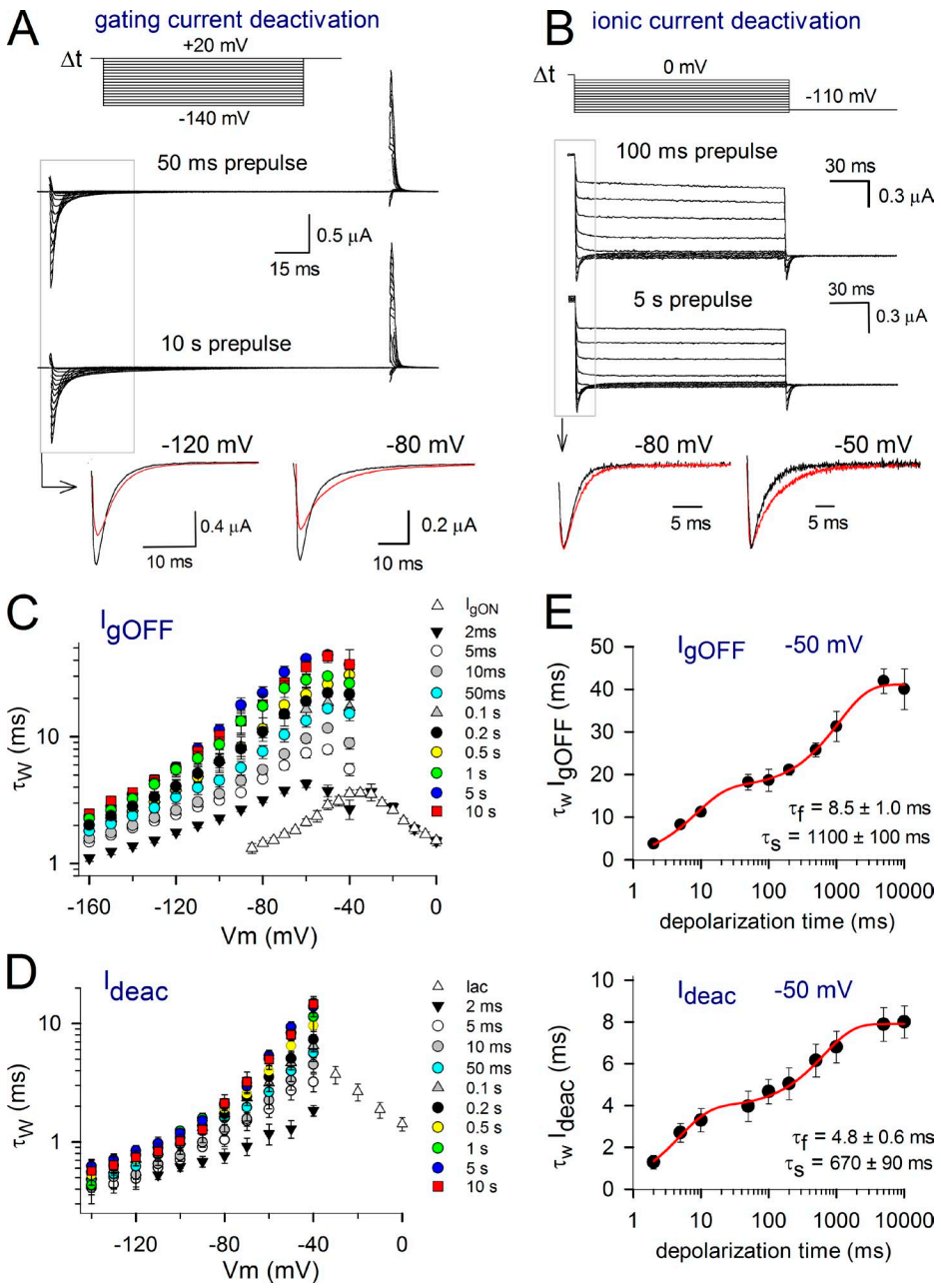

Figure 2. Slowing in I_{gOFF} and I_{deac} kinetics of *Shaker* channels with prolonged depolarization. (A) Deactivating I_{gOFF} currents upon different depolarization times at 20 mV. To avoid nonspecific effects or depletion effects, the pulse protocols were ran in random order, and, in the case of the represented currents, the protocol with a 10-s prepulse (bottom traces) was recorded before the 100-ms trace (top traces). (bottom) A superposition of I_{gOFF} at different voltages upon 100-ms (black) and 10-s depolarizations (red). Note that I_{gOFF} slows down and the total charge becomes more spread out when depolarizations are prolonged. (B) Ionic current deactivation after 100 ms (top traces) and 5 s (bottom traces) at 20 mV. (bottom) A superposition of scaled currents at −80 and −50 mV upon 100-ms (black) and 5-s (red) depolarizations. (C) I_{gOFF} was fitted with a double exponential function, and the weighted time constants ± SEM are represented ($n = 6$). Note the gradual increase of the time constants with prolonged depolarization times. (D) Development of the ionic deactivation I_{deac} weighted time constant as a function of depolarization time, displaying, like I_{gOFF}, a gradual slowing with prolonged depolarizations. (E, top) The weighted I_{gOFF} time constant at −50 mV plotted as a function of depolarization time clearly displaying two slowing processes. The fit with a double exponential function yielded a fast τ_f of 8.5 ± 1.0 ms and a slow τ_s of 1,100 ± 100 ms ($n = 6$). (bottom) The behavior of I_{deac} kinetics at −50 mV showing a similar biphasic slowing process with a τ_f of 4.8 ± 0.6 ms and a τ_s of 670 ± 90 ms ($n = 5$). Error bars represent SEM.

The time constant of the Ig_{ON} decays matched the time constant of ionic current activation I_{ac} that directly reflects the opening of the BC gate (Fig. 1, A, B, and F). In accordance with a previous study, the ionic current deactivation I_{deac} was analyzed with a double exponential function yielding a fast and a slow component (Stefani et al., 1994). To correlate I_{gOFF} and I_{deac} correctly, the kinetics of both were analyzed pairwise in the same oocyte (Fig. 1, D and E). It is well established that the rate of decay of Ig_{OFF} decreases as the amplitude of the depolarizing prepulse increases and exceeds the threshold for opening the BC gate (about −50 mV for *Shaker*; Fig. 1 B; Hoshi et al., 1990; Bezanilla et al., 1994). Concomitantly with this slowing, Ig_{OFF} displays an unambiguous rising phase that is presumably caused by the stabilization of the conducting conformation of the channels (Batulan et al., 2010). The direct pairing analysis shows that the fast component of the I_{deac} kinetics matched the time course of the rising phase in I_{gOFF} (Fig. 1, E and F). This rising phase reflects an initial rate-limiting energy barrier for the deactivation VSD transition coming from its activated state. As shown previously, the slow component in I_{deac} followed Ig_{OFF} decay (Fig. 1, E and F; Bezanilla et al., 1991). Apparently, the fast I_{deac} component had the largest contribution in the overall process of channel closure, which is reflected in the weighted average I_{deac} kinetics (Fig. 1 F).

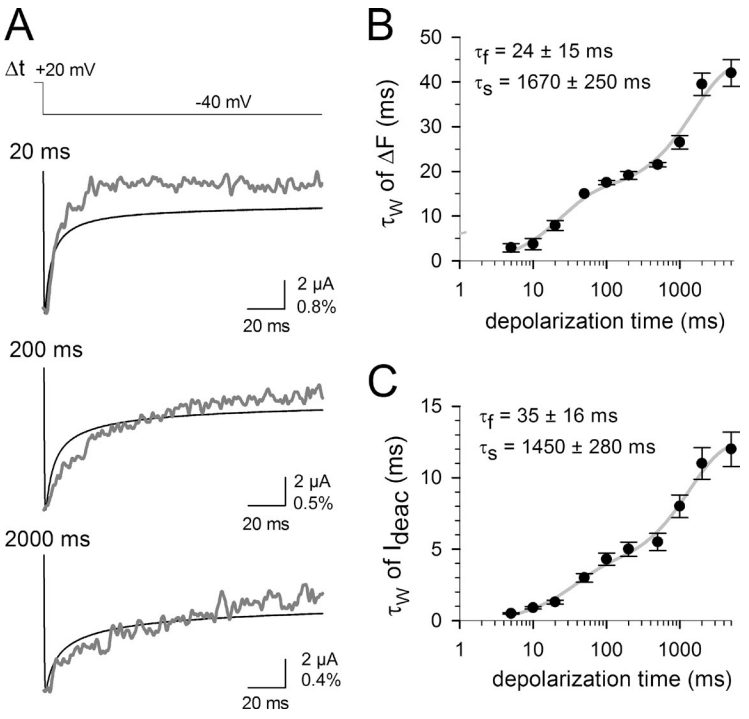

Figure 3. Direct correlation between VSD and gate movement in the *Shaker*-M356C channel using site-directed fluorimetry. (A) Simultaneous recording of I_{deac} (black traces) and recovery of fluorescence quenching (ΔF, gray traces) from an oocyte expressing TMRM-labeled M356C *Shaker* channels using the indicated protocol and various prepulse durations at 20 mV. For clarity, both traces have been normalized. The vertical scale bar indicates both ionic current amplitude (in microamps) and ΔF/F (in percentage). (B) The kinetics of the fluorescence recovery signal obtained at −60 mV is shown as a function of the prepulse duration. Note that like the gating current recordings, there were two slowing process in the kinetics with prolonged membrane depolarizations. (C) Development of the weighted I_{deac} time constant at −60 mV as a function of depolarization time, displaying, like the simultaneously recorded ΔF signal, a biphasic slowing of the kinetics. Error bars represent SEM.

Synchronized slowing in I_{gOFF} and I_{deac} kinetics in *Shaker* upon prolonged membrane depolarizations

We previously showed that the overall kinetics of deactivating gating currents in *Shaker* channels displays a biphasic slowing down upon prolonged depolarizations (Fig. 2 A; Lacroix et al., 2011). Similarly, our present analysis of I_{gOFF} with varying durations of depolarization showed that there were two noticeable slowing phases (Fig. 2, C and E). The fast developing slowing process developed with a time constant τ_f of 8.5 ± 1.0 ms and has been linked to the stabilizing interaction imposed by pore opening (Kanevsky and Aldrich, 1999; Batulan et al., 2010). The second, slower developing slowing period had a time constant τ_s of 1,100 ± 100 ms, which corresponds to the VSD relaxation (Lacroix et al., 2011).

As there seems to be a strong correlation between the gating and ionic current kinetics, the time constant of I_{deac} is expected to also increase upon prolonged depolarizations. In agreement with the slowing in VSD return, there appeared a slow decaying I_{deac} component that gradually increased in amplitude when the depolarization prepulse durations were prolonged (Fig. 2 B). Similar to the I_{gOFF} behavior, there were two distinct slowing processes in I_{deac} kinetics (Fig. 2, D and E). The first, a fast developing process, occurred within a time window of 20 ms and most likely reflects the open pore stabilization process that occurs upon channel opening. The speed of channel closure slowed down further upon prolonged depolarizations, reaching a steady-state maximal value with prepulse durations of 5 s or longer. Plotting the I_{deac} kinetics at −50 mV as a function of depolarization time showed that the two slowing processes, with a τ_f of 4.8 ± 0.6 ms and a τ_s of 670 ± 90 ms (n = 5), were similar to the slowing processes in I_{gOFF}. Moreover, upon the first and second slowing process, both I_{gOFF} and I_{deac} kinetics increased by a factor of four and a factor of two, respectively (Fig. 2 E). Thus, as both the time development and the magnitude of the slowing process in I_{gOFF} and I_{deac} were similar, both processes appeared to be well correlated.

Because differences in recording conditions for ionic and gating current measurements might have affected the observed slowing processes in I_{gOFF} and I_{deac} kinetics, we monitored VSD and BC gate movements simultaneously using site-directed fluorimetry (Cha and Bezanilla, 1997). To achieve this, we covalently attached the conformational reporter TMRM to a cysteine inserted at the top of S4 (M356) in *Shaker* channels. This allowed us to simultaneously record the changes in fluorescence (ΔF) that report on the VSD movements and the amplitude and kinetics of the ionic currents reflecting opening/closure of the BC gate. Fig. 3 A shows examples of I_{deac} and recovery in ΔF traces during repolarizing pulses to −40 mV after prepulses of variable durations to 20 mV. The time constants of both I_{deac} and ΔF were calculated and plotted as a function of the depolarization duration, and the results show an identical biphasic slowing for both I_{deac} and ΔF (Fig. 3, B and C). The first slowing developed with a τ_f of 35 ± 16 ms for I_{deac} and 24 ± 15 ms for ΔF, and the second one had a τ_s of 1,450 ± 280 ms for I_{deac} and 1,670 ± 250 ms for ΔF (n = 5; the slowing processes in I_{deac} are slower here than in WT *Shaker*, presumably because of the presence of the

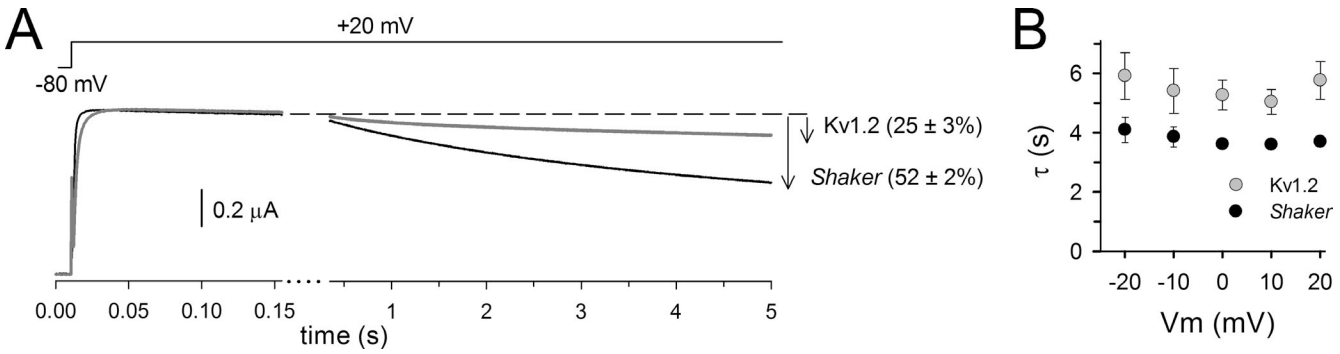

Figure 4. C-type inactivation properties of *Shaker* and Kv1.2. (A) Ionic current recordings from oocytes expressing *Shaker* (black trace) or Kv1.2 channels (gray trace) evoked by depolarizing the membrane potential from a holding of −80 to 20 mV. Upon prolonged depolarization, both channels display C-type inactivation, which is characterized by a reduction in current amplitude. At the end of the pulse, Kv1.2 channels display only 25 ± 3% ($n = 4$) current reduction, whereas *Shaker* channels display 52 ± 2% current decrease ($n = 4$). (B) Time constants of the inactivation process in *Shaker* (black circles) and Kv1.2 channels (gray circles) obtained by fitting the reduction in current amplitude with a single exponential function. Note that in both channels, the kinetics are voltage independent. Error bars represent SEM.

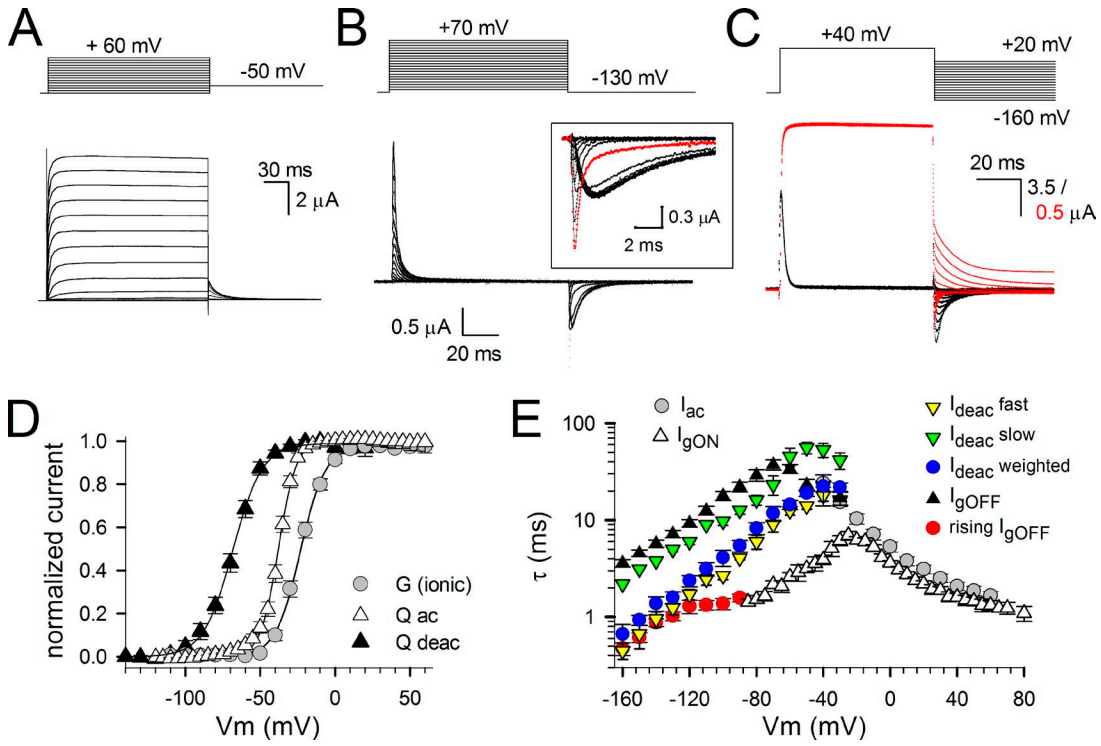

Figure 5. Ionic and gating currents from Kv1.2; behavior of the VSD and BC gates. (A) Activating ionic currents from WT Kv1.2, a member of the *Shaker* family that displays a more modest C-type inactivation process. (B) Gating current recordings from Kv1.2 after depletion of K^+. Current recordings were obtained using the activation pulse protocol shown on top. The holding potential was −130 mV, and oocytes were depolarized in 5-mV increments from −130 to 70 mV (for clarity only, current traces are shown every 10-mV increment). Similar to *Shaker*, there was a gradual slowing in I_{gOFF} decay when prepulse depolarization voltages became stronger (red trace is I_{gOFF} after a −40-mV prepulse). (C) Superposition of scaled deactivation ionic (red traces) and gating currents (black traces) from Kv1.2 obtained from the same oocyte using the voltage protocol shown on top. The scales for gating and ionic currents are shown in black and red, respectively. (D) Voltage dependence of BC gate opening (GV curve) and charge movement (QV curves) using an activation (Q_{ac}) or deactivation (Q_{deac}) protocol. Both GV and QV values were normalized, and for both GV and QV curves, the average fit to a Boltzmann equation is shown. (E) Mean time constant ± SEM for I_{gON} decay (open triangles), I_{gOFF} decay (closed triangles), rising phase of I_{gOFF} (red circles), I_{ac} (gray circles), fast component of I_{deac} (yellow inverted triangles), slow component of I_{deac} (green inverted triangles), and the weighted I_{deac} kinetics (blue circles) obtained in a similar way as described for *Shaker* (Fig. 1), with an n of at least six independent oocytes analyzed. Error bars represent SEM.

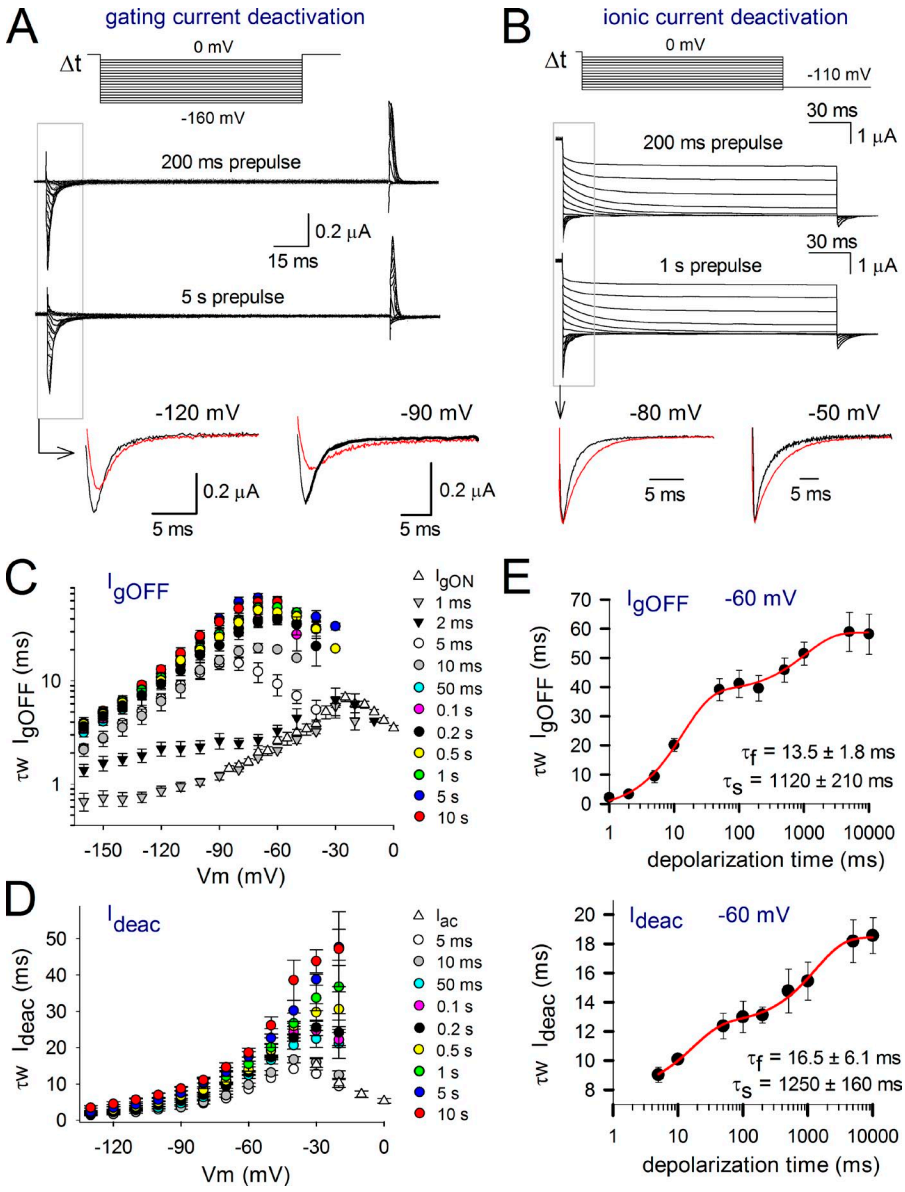

Figure 6. Slowing in I_{gOFF} and I_{deac} kinetics of Kv1.2 with prolonged depolarization times. (A) Deactivating gating (I_{gOFF}) currents upon 200-ms (top traces) and 5-s (bottom traces) prepulse depolarization times at 20 mV. Like the experiments on *Shaker*, the pulse protocols were ran in random order to avoid nonspecific effects on channel kinetics. (bottom) A superposition of I_{gOFF} at −120 and −90 mV upon 200-ms (black) and 5-s (red) depolarizations, respectively. (B) Ionic current deactivation after 200 ms (top traces) and 1 s (bottom traces) at 20 mV. (bottom) A superposition of scaled ionic currents at −80 and −50 mV upon 200-ms (black) and 1-s (red) depolarizations. (C) I_{gOFF} kinetics as a function of depolarization duration at 20 mV. Values were obtained by weighting the time constants from a double exponential fit to I_{gOFF} decay at different voltages ($n = 5$). (D) Voltage dependence of BC gate closure (I_{deac}) as a function of depolarization duration at 20 mV. The weighted I_{deac} kinetics obtained from a double exponential fit ± SEM ($n = 7$) are plotted. (E, top) The weighted I_{gOFF} kinetics at −60 mV as a function of prepulse depolarization time. Like *Shaker*, there were two noticeable slowing processes in I_{gOFF} kinetics, a fast τ_f of 13.5 ± 1.8 ms and a slow τ_s component of 1,120 ± 210 ms ($n = 5$). (bottom) Plot of the development of the weighted I_{deac} kinetics as a function of prepulse depolarization time. Like I_{gOFF}, there appeared two clear slowing processes, and fitting the relation with a double exponential function yielded a τ_f of 16.5 ± 6.1 ms and a τ_s of 1,250 ± 160 ms ($n = 7$). Error bars represent SEM.

TMRM linked at M356C). This confirms that the VSD and BC gate movements are strongly coupled and that both VSD return and BC gate closure slow down upon VSD relaxation.

Kv1.2 channels display a similar VSD and BC gate behavior with prolonged depolarizations

The aforementioned results indicated that in *Shaker* channels, the VSD gets stabilized in an upward conformation (relaxed state) by spending longer periods at depolarizing potentials. It is conceivable that a similar mechanism exists in other Kv channels such as Kv1.2. Although Kv1.2 is a mammalian homologue of the bigger *Shaker* subfamily of Kv channels and thus shares a high sequence homology, both *Shaker* and Kv1.2 differ in their C-type inactivation process (Stühmer et al., 1989; Hoshi et al., 1990; Ramaswami et al., 1990). Fig. 4 shows that after a 5-s activation pulse to 20 mV, approximately half of the *Shaker* channels have entered their inactivated state, whereas only a quarter of Kv1.2 channels were inactivated. Moreover, the time course of the inactivation of the potassium conductance in these two channels differs with time constants of ∼3.5 s in *Shaker* and 5.5 s in Kv1.2, respectively. Because of these differences in C-type inactivation, we wondered whether prolonged depolarizations affect the VSD deactivation and BC gate closure of Kv1.2 channels in a similar or distinct manner compared with *Shaker*.

To test this, we recorded gating and ionic currents from WT conducting Kv1.2 channels (Fig. 5, A–C). The voltage dependence of charge movement during activation resulted in a QV curve with a midpoint potential of −37.9 ± 1.0 mV and slope factor of 5.9 ± 0.6 mV ($n = 6$; Fig. 5 D). The GV curve had a midpoint of −23.3 ± 2.6 mV

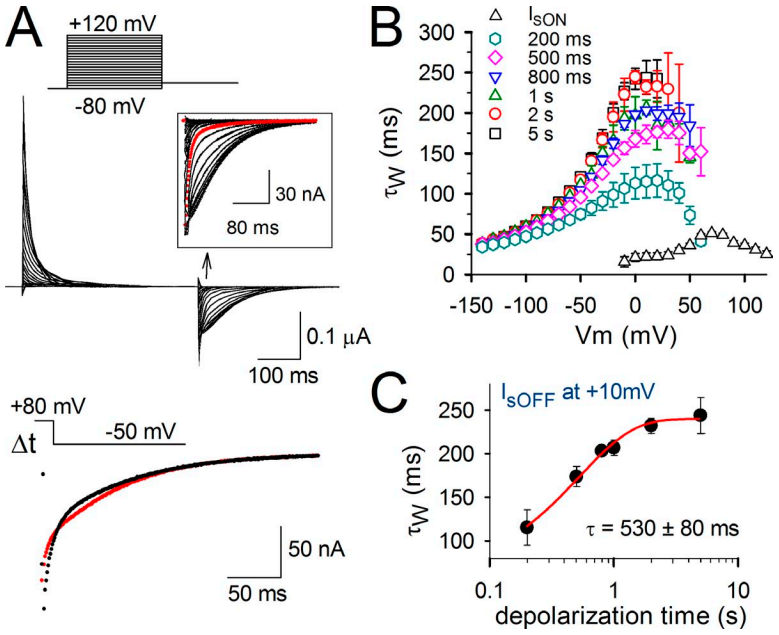

Figure 7. Slowing in charge return of Ci-VSP sensing current I_s. (A, top) Current tracings showing I_s of Ci-VSP using the indicated activation protocol. The I_{sOFF} from a moderate 30-mV test pulse is shown as the red trace in the inset. Note the rapid slowing down in Is_{OFF} that accompanies the most positive depolarizations. (bottom) Current tracings are a superposition of I_{sOFF} at −50 mV upon 200-ms (black) and 1-s (red) depolarizations to 80 mV. Note the slowing in I_{sOFF} decay when depolarizations get prolonged. (B) Kinetics of activating I_{sON} (open triangles) obtained in WT Ci-VSP from different activation voltage pulses (similar to the protocol shown in A) and of deactivating I_{sOFF} obtained in WT Ci-VSP using 80-mV prepulses of the indicated durations from 200 ms to 5 s (colored symbols) and pulsing to different deactivation voltages. (C) The weighted time constant of I_{sOFF} decay measured at 10 mV is plotted as a function of the duration of the conditioning prepulse. The obtained curve was fitted to a single exponential function and yielded a time constant of $\tau = 530 \pm 80$ ms ($n = 7$). Error bars represent SEM.

with a slope factor of 7.9 ± 0.5 mV ($n = 9$), i.e., ∼10 mV displaced to more positive potentials compared with the QV curve. Furthermore, the voltage dependence of gating charge deactivation, determined from integrating I_{gOFF} using a deactivation protocol (Fig. 5 C), resulted in a QV curve with a midpoint of −68.3 ± 2.0 mV and a slope factor of 9.8 ± 1.0 mV ($n = 5$), which is ∼30 mV more negative than the QV curve obtained from an activation protocol (Fig. 5 D). Thus, the underlying relation between the GV and QV curves was in Kv1.2 quite similar to *Shaker*. The time constants of I_{gON}, I_{gOFF}, I_{ac}, and I_{deac} were obtained with the same procedure as described previously (see section Strong correlation between VSD movement. . .) for *Shaker* (Fig. 5 E). Likewise, the I_{ac} time constants nicely matched the I_{gON} kinetics, and the slow component of I_{deac} matched the decay in I_{gOFF} well. In addition, the fast component of I_{deac} followed the rising phase in I_{gOFF} and, as in *Shaker*, appeared to contribute most to the overall ionic current deactivation, as shown by the weighted average I_{deac} kinetics (Fig. 5 E).

Investigating the I_{gOFF} behavior as a function of the depolarizing prepulse duration indicated that there were two noticeable slowing phases (Fig. 6). As for *Shaker*, the first slowing followed BC gate opening and most likely results from a similar stabilizing $S4S5_L$–S6 interaction (Batulan et al., 2010). More importantly, the second slowing starts to develop for durations that exceed steady-state BC gate opening (Fig. 6 E). Therefore, this second slowing in I_{gOFF} indicated that the VSD of Kv1.2 becomes stabilized in a secondary activated (relaxed) state upon prolonged depolarizations. We determined the time course for the development of this slowing down in the I_{gOFF} kinetics by fitting the I_{gOFF} traces at −60 mV with a double exponential function. The fit yielded a τ_f of 13.5 ± 1.8 ms and a τ_s of 1,120 ± 210 ms ($n = 5$; Fig. 6). The analysis of the kinetics of I_{deac} showed that BC gate closure also slows down and displays two slowing periods with a τ_f of 16.5 ± 4.1 ms and a τ_s of 1,250 ± 160 ms ($n = 7$; Fig. 6). Consequently, the development of both slowing processes in I_{deac} and I_{gOFF} appeared very well synchronized. Furthermore, during the second slowing process, which produces a 1.5-fold slowing down in both I_{gOFF} and I_{deac} (Fig. 6), Kv1.2 channels display only ∼25% of C-type inactivation.

VSD relaxation is an intrinsic property of the VSD

Negative shifts in the QV curve determined from activation or deactivation gating currents have been ubiquitously reported in voltage-sensitive proteins. It is thus tempting to raise the hypothesis that these QV shifts are apparent as a result of a VSD relaxation process similar to Kv channels. Accordingly, the relaxation would be an intrinsic property of a VSD with a four-transmembrane topology, and it would not be allosterically triggered by another region of the protein. To test this hypothesis, we investigated VSD relaxation in Ci-VSP, which does not contain a pore (Fig. 7). As reported previously, the kinetics of the deactivating sensing current (Is_{OFF}; Fig. 7 A) undergoes a relatively rapid slowing down upon strong depolarizing pulses, a phenomenon that has been attributed to the binding of the phosphatase domain to the membrane (Villalba-Galea et al., 2009). However, analyzing the effect of prolonged prepulse durations revealed a second gradual slowing in Is_{OFF} decay time, similar to *Shaker* and Kv1.2 channels (Fig. 7, B and C). A shift in the QV curve of Ci-VSP sensing currents has been reported previously (Villalba-Galea et al., 2008), and, as we show here, this shift may be mostly apparent as a result of a slowing in the deactivation kinetics of VSD return (relaxation process).

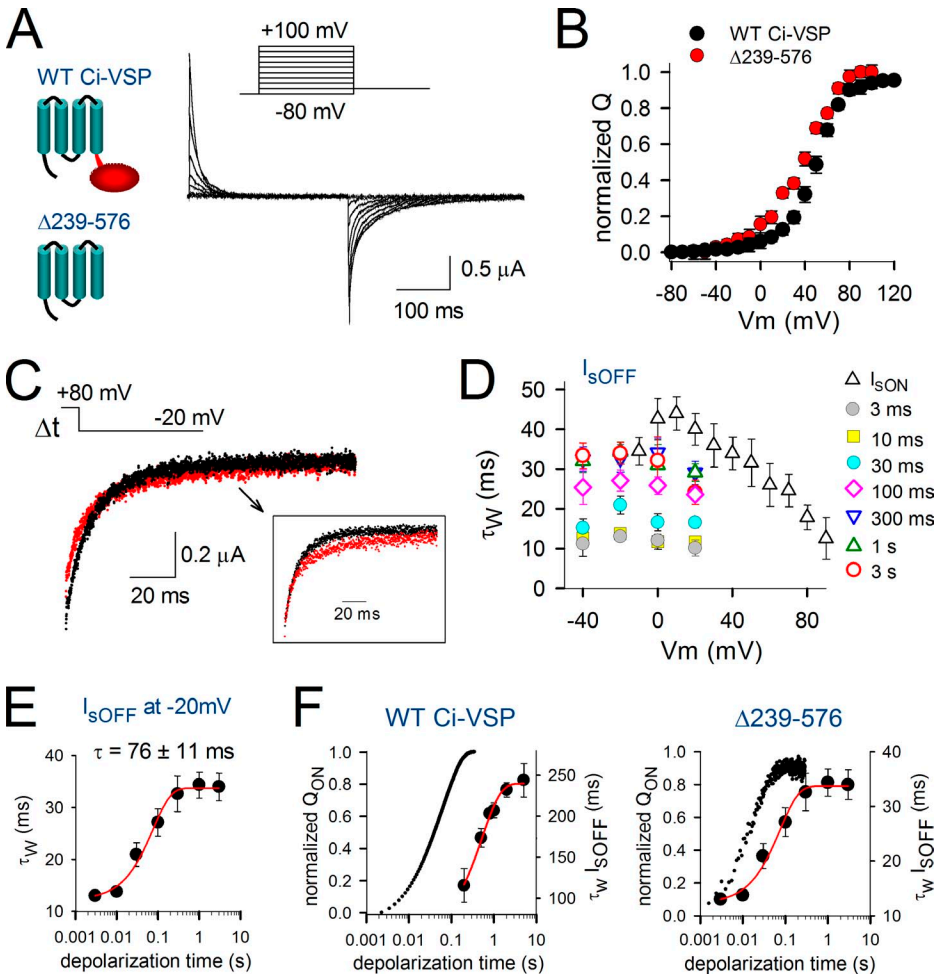

Figure 8. VSD relaxation in the isolated VSD of Ci-VSP. (A, left) Cartoon representation of the full-length WT Ci-VSP and the truncated mutant Δ239–576 that lacks the phosphatase domain (red) attached to the VSD (blue). (right) Sensing current traces (I_s) of the truncation mutant Δ239–576 recorded using the indicated activation protocol. (B) QV curves for the mutant Δ239–576 (red) and WT Ci-VSP (black) obtained by integrating the activating I_s from pulse protocols shown in A and Fig. 7 A, respectively. (C) A superposition of I_{sOFF} current traces at −20 mV after 10-ms (black) and 3-s (red) depolarizations to 80 mV is displayed. Note the slowing in I_{sOFF} decay and the reduction in the fast component amplitude of the red trace. The inset shows the normalized tracings to better highlight the slowing in I_{sOFF} decay. (D) Kinetics of activating I_{sON} (open triangles) of the mutant Δ239–576 obtained from different activation voltage pulses (similar to the protocol shown in A) and of deactivating I_{sOFF} of the same mutant obtained using 80-mV prepulses of the indicated durations from 3 ms to 3 s (colored symbols) and pulsing to different deactivation voltages. (E) Weighted time constant of I_{sOFF} decay measured at −20 mV as a function of the duration of the conditioning prepulse at 80 mV. The obtained curve was fitted to a single exponential function and yielded a time constant of τ = 76 ± 11 ms (n = 5). (F) For both the full-length Ci-VSP (left) and the truncation mutant Δ239–576 (right), the normalized amount of sensing charges moved during the conditioning prepulse to 80 mV (Q_{ON}, left axis) was superimposed on the depolarization-induced slowing in the kinetics of I_{sOFF} decay ($\tau_w I_{sOFF}$, right axis). Fitting the normalized charge displacement as a function of depolarization duration with a single exponential function yielded τQ_{ON}^{WT} = 61.7 ± 0.1 ms (n = 4) for full-length Ci-VSP and $\tau Q_{ON}^{\Delta 239-576}$ = 18.8 ± 0.1 ms (n = 5) for the truncation mutant. Error bars represent SEM.

To investigate the VSD relaxation in the absence of any load attached to the S4 helix, we created the Ci-VSP truncation mutant Δ239–576 by removing the entire phosphatase domain (Fig. 8 A). This mutant displayed a voltage dependence of sensing current activation that was slightly shifted toward more negative potentials compared with full-length Ci-VSP (Fig. 8, A and B). The maximal value of Is_{OFF} for the deletion mutation was obtained upon repolarizing to −20 mV instead of 10 mV for the WT Ci-VSP (Fig. 8, C and D). By comparing the maximal values of Is_{OFF}, we found that they decayed ∼10-fold faster in the truncated Δ239–576 mutant compared with the full-length Ci-VSP ($Is_{OFF}^{\Delta 239-576}$ = 13 ± 1 ms vs. Is_{OFF}^{WT} = 115 ± 20 ms for short prepulses and $Is_{OFF}^{\Delta 239-576}$ = 34 ± 3 ms vs. Is_{OFF}^{WT} = 244 ± 21 ms for long prepulses; compare Fig. 7 B with Fig. 8 D). Despite this acceleration, the decay kinetics of Is_{OFF} slowed down with increased prepulse depolarization time similar to the full-length Ci-VSP. However, the time course of VSD relaxation in the truncated mutant appeared to be accelerated compared with the full-length version and developed with a time constant of 76 ± 11 ms (n = 5) at 80-mV depolarization. This is about sevenfold faster than the full-length version whereby relaxation developed with a time constant of 530 ± 80 ms (Fig. 7 C).

To confirm that the slowing in Is_{OFF} occurred subsequently to the charge movement during activation, we determined for both the full-length Ci-VSP and the Δ239–576 mutant the time course of the sensing charge movement during the depolarizing prepulse by integrating Is_{ON}. The truncation of the phosphatase domain appeared to accelerate threefold the sensing charge displacement at 80 mV (τQ_{ON}^{WT} = 61.7 ± 0.1 ms compared with $\tau Q_{ON}^{\Delta 239-576}$ = 18.8 ± 0.1 ms), yet there was (as in the full-length Ci-VSP) a clear temporal delay between the displacement of the sensing charge and the slowing

process in Is_{OFF} ($\tau Q_{ON}^{\Delta 239-576}$ = 18.8 ± 0.1 ms vs. $\tau_{relaxation}^{\Delta 239-576}$ = 76 ± 11 ms; Fig. 8 D). Because the Is_{OFF} kinetics of the deletion mutant slowed down from 13 ± 1 to 34 ± 3 ms (Fig. 8 C), the extent of the slowing was comparable to the two- to threefold slowing observed in WT Ci-VSP, *Shaker*, and Kv1.2. Thus, the truncation mutant displayed the characteristic relaxation that developed subsequently to sensing charge displacement. This indicates that the isolated VSD from Ci-VSP is able to undergo relaxation in the absence of any load at the C-terminal end of the S4 segment.

DISCUSSION

Direct pairing of VSD movement with BC gate opening/closure in *Shaker* and Kv1.2 channels showed that in both channels, the time course of ionic current activation (I_{ac}) followed that of I_{gON} decay. This indicates that BC gate opening arises late in the activation sequence and is linked to one of the final transition steps of the VSD. This is in agreement with previous proposed gating schemes for the *Shaker* channel (Bezanilla et al., 1994; Zagotta et al., 1994; Schoppa and Sigworth, 1998) in which BC gate opening requires that all four VSDs have moved to the preactivated/activated state. I_{deac} displayed two components, and, in agreement with a previous study, the late one followed I_{gOFF} decay (Bezanilla et al., 1991). The fast component in I_{deac}, as we show here, followed the rising phase in I_{gOFF}, indicating that it is linked to a first rate-limiting transition in the sequential steps of VSD return (Fig. 1).

The slowing in the deactivation kinetics of the gating (I_{gOFF}) and ionic (I_{deac}) currents in both *Shaker* and Kv1.2 displayed two identifiable phases, a fast developing one and a slower one (Figs. 2 and 6). It has been shown that the fast developing slowing in I_{gOFF} kinetics is linked to channel opening (Kanevsky and Aldrich, 1999; Batulan et al., 2010). Remarkably, however, there was a similar slowing in BC gate closure (I_{deac}) that developed within the same time window. This indicates that the slowing in VSD return or BC gate closure is not established immediately after channel opening. A recent study showed that this fast developing slowing in I_{gOFF} kinetics, linked to BC gate opening, is caused by the establishment of intersubunit interactions between specific residues of the $S4S5_L$ and C-terminal S6 (S6c) segment that stabilize the VSD in the active state (Batulan et al., 2010). As shown by Batulan et al. (2010), the disruption of these interactions alleviates the rapid slowing in Ig_{OFF} but does not prevent BC gate opening. This is in agreement with our observation of a time lag between BC gate opening and the establishment of the stabilizing $S4S5_L$–S6c interactions that results in a slowing of both I_{gOFF} and I_{deac} kinetics.

After this initial slowing, there appeared a subsequent second slowing down in VSD return and BC gate closure when the membrane depolarization was prolonged beyond the duration of the charge movement. Similar to the first process, this second slowing phase in I_{gOFF} and I_{deac} kinetics was synchronized, as further indicated by our site-directed fluorimetry data from the *Shaker*-M356C mutant (Fig. 3). Because the first stabilization is caused by an $S4S5_L$–S6c interaction, one might argue that a similar pore stabilization also accounts for this second slowing process. Recently, Haddad and Blunck (2011) showed that mutations within $S4S5_L$ (I358N) and S6c (F484G) that uncouple the communication between the VSD and pore domain prevented this second slowing period in I_{gOFF} kinetics. However, both their data and our data indicate that the coupling between the VSD and BC gate is very tight and mutations within the pore module will consequently affect the transition rate toward the channel's relaxed state. These data cannot rule out the hypothesis that this second VSD stabilization (the relaxation process) is an intrinsic property of membrane proteins possessing an S4-based VSD. In fact, the relaxation process, being an intrinsic property of the VSD, is strengthened by our observation that Ci-VSP, which does not contain a pore domain, and even its isolated VSD display a similar slowing in VSD return as a function of the time spent in the activated state (Figs. 7 and 8). We propose that this second slowing in the kinetics of BC gate closure (I_{deac}) and VSD deactivation (I_{gOFF}) in *Shaker* and Kv1.2 channels is the direct consequence of a stabilization of the VSD into its relaxed state.

Although we do not rule out that the conformational changes of the pore when entering the C-type inactivated state have an impact on the movement of the VSD, our data strongly support that the described modulation in I_{gOFF} and I_{deac} kinetics occurs independently from the state of the K^+ selectivity filter (being conductive or inactivated). First, the process of VSD relaxation is also observed in Ci-VSP and its isolated VSD version (Figs. 7 and 8). Second, the gating currents were recorded from conducting *Shaker*-H4-IR by depletion of potassium, and it has been described that reducing the K^+ flux speeds up C-type inactivation substantially (Baukrowitz and Yellen, 1995, 1996; Starkus et al., 1997). Consequently, the slowing in I_{gOFF} (K^+-depleted conditions) and I_{deac} (recorded in the presence of K^+) would not be synchronized if C-type inactivation was involved. Moreover, I_{deac} reports only from noninactivated channels, whereas Ig_{OFF} reports from both inactivated and noninactivated channels. Thus, if C-type inactivation were to affect the return of the VSD, there should be a discrepancy between the time-dependent changes in the kinetics of these two types of currents, which was not the case. Third, we recently showed that *Shaker*-W434F, a channel mutant that displays extremely fast inactivation (Yang et al., 1997), displays I_{gOFF} slowing with a similar time development (Lacroix et al., 2011).

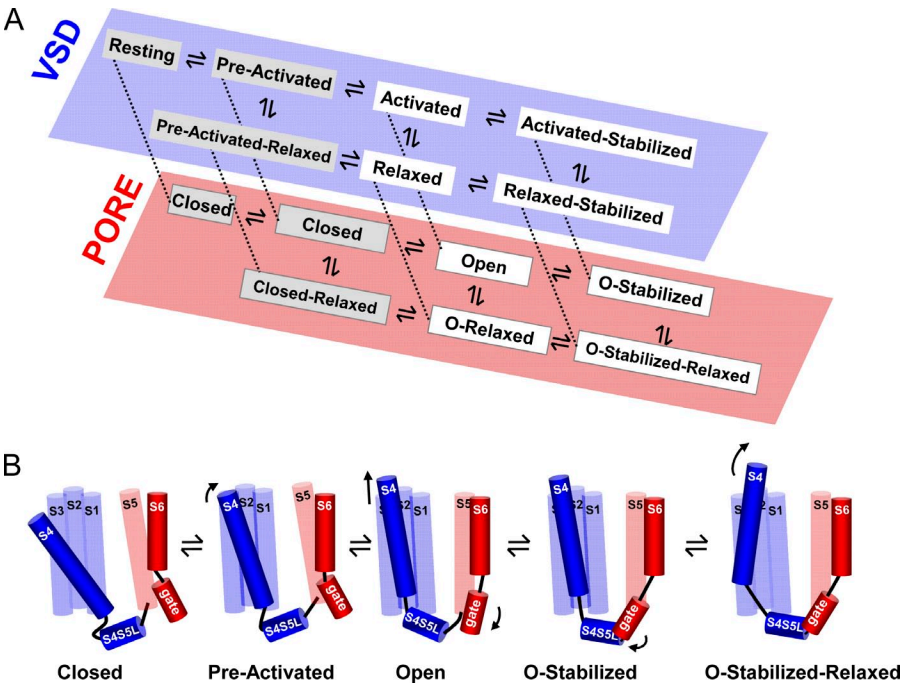

Figure 9. State model and cartoon of the activation path in *Shaker* and Kv1.2. (A) Proposed simplified state diagram for *Shaker* and Kv1.2 channels whereby the state occupancy for both VSD (blue) and BC (red) gates are represented in two separate schemes. The stabilization imposed by the BC gate is termed the open stabilized (O-stabilized) state and results in the activated stabilized state at the VSD level. The stabilization that originates from the VSD relaxation process results in the relaxed and open relaxed (O-relaxed) state of the VSD and BC gate, respectively. (B) Cartoon of the structural path followed by *Shaker* and Kv1.2 channels upon a membrane depolarization. For clarity, only one out of four subunits is illustrated, and the specific change from one state to the next is indicated by an arrow. During a depolarization, the VSD (mostly the S4 segment) moves from its resting position (at the extreme left) to its preactivated state and in a subsequent concerted step to its activated state, resulting in the opening of the BC gate (open). Because in *Shaker* and Kv1.2 the stabilization imposed by the BC gate (depicted by the interaction between the $S4S5_L$ and S6 gate region) develops first, the BC gate evolves from the open to the open stabilized (O-stabilized) conformation. When the depolarization is prolonged, the VSD relaxes (illustrated with a tilt of the S4), and the channel populates its final open stabilized relaxed (O-stabilized-relaxed) state.

Fourth, Kv1.2 channels whose C-type inactivation develops markedly slower than in *Shaker* channels (Fig. 4) displayed a VSD relaxation similar to *Shaker* channels. Finally, in both *Shaker* and Kv1.2 channels, the rate of C-type inactivation is approximately three- to fivefold slower than the time course of the VSD relaxation process.

Although the exact underlying molecular mechanism for VSD relaxation is at present unknown, it involves a stabilization of the VSD in a postactivated conformation. Because of the strong coupling with the BC gate, this VSD relaxation is also reflected in the speed of gate closure. A previous study in hKv1.5 channels (the closest human homologue of *Shaker*) reported a similar slowing down in I_{deac} kinetics when depolarization times were increased (Rich and Snyders, 1998). Furthermore, as there were good reasons to conclude that this slow component in I_{deac} did not arise from channels recovering from an underlying hidden inactivated state, Rich and Snyders (1998) interpreted their observation as the channel having multiple open configurations. From the point of view of the kinetics of K^+ conductance, this is indeed the case, but we show here that the underlying cause is the VSD relaxation process, and, therefore, the structural conformation of the BC gate might be similar in both open states.

Based on our previously described kinetic model that accounts for VSD relaxation at the level of gating charge movement and the observation that there is a tight coupling with the BC gate, we propose a gating scheme for both *Shaker* and Kv1.2 channels that accounts for the biphasic slowing process observed in both deactivating gating (I_{gOFF}) and ionic (I_{deac}) currents (Fig. 9 A). To adequately illustrate the stabilizing effect of relaxation on both VSD deactivation and BC gate closure, we show two parallel schemes, one reflecting the status of the VSD and the other the BC gate. Both schemes are interconnected such that a stabilizing state in one scheme will result in a stabilized state in the other. Although the represented state model follows a square pathway occupying different energetic states, the forward and backward path followed by the VSD and BC gate can be structurally the same. Therefore, we provide an illustration of a linear scheme for the structural rearrangements in *Shaker* and Kv1.2 channels as a function of depolarization history (Fig. 9 B). Upon membrane depolarization, the channels evolve from closed over a preactivated state to the open state. Subsequently, there is a first stabilization imposed by the BC gate, and when depolarization is maintained, the VSD rearranges, resulting in a second stabilization referred to as the open relaxed state. This illustration concurs with the biphasic slowing observed in both I_{gOFF} and I_{deac}, indicating the existence of three identifiable open channel conformations.

Because depolarization-induced QV shifts have been ubiquitously observed among various voltage-dependent proteins containing an S4-based VSD (Bezanilla et al., 1982; Shirokov et al., 1992; Piper et al., 2003; Kuzmenkin

et al., 2004; Männikkö et al., 2005; Bruening-Wright and Larsson, 2007; Villalba-Galea et al., 2008; Xiao et al., 2010), this phenomenon called VSD relaxation is a general behavior of the VSD, but the time frame over which it develops and the impact of the process on the gating kinetics may differ.

In vivo Kv channels contribute to the repolarizing power that terminates the action potential and determines cell excitability at resting conditions. Whereas C-type inactivation results in a decrease in K^+ conduction, thus reducing the repolarizing power, slowing down channel closure has the opposite effect. Therefore, both processes affect the excitability of cells differently, and, in the case of *Shaker*, in which both occur simultaneously, they may counteract each other. However, in Kv1.2 channels in which C-type inactivation develops slower than VSD relaxation, the slowing in BC gate closure may have a physiological impact, as it occurs while the selectivity filter remains highly conductive.

The crucial role played by Kv1.2 channels in controlling repetitive firing of a large variety of neurons has been well established (Glazebrook et al., 2002; Dodson et al., 2003; Shen et al., 2004; Khavandgar et al., 2005; Brew et al., 2007; Douglas et al., 2007; Shu et al., 2007; Xie et al., 2010). We propose here that VSD relaxation, a ubiquitous property of the VSD, may constitute the physiological mechanism that enables slowing down of BC gate closure in Kv1.2 channels.

This research was funded by National Institutes of Health grant GM030376 (to F. Bezanilla), the Research Foundation Flanders, grants G.0256.08 (to D.J. Snyders) and 1.5.087.11N (to A.J. Labro), and grant GOA/TOP41.3016 from the concerted action fund of the University of Antwerp.

Kenton J. Swartz served as editor.

Submitted: 12 April 2012
Accepted: 13 September 2012

REFERENCE LIST

Batulan, Z., G.A. Haddad, and R. Blunck. 2010. An intersubunit interaction between S4-S5 linker and S6 is responsible for the slow off-gating component in Shaker K+ channels. *J. Biol. Chem.* 285:14005–14019. http://dx.doi.org/10.1074/jbc.M109.097717

Baukrowitz, T., and G. Yellen. 1995. Modulation of K+ current by frequency and external [K+]: a tale of two inactivation mechanisms. *Neuron.* 15:951–960. http://dx.doi.org/10.1016/0896-6273(95)90185-X

Baukrowitz, T., and G. Yellen. 1996. Use-dependent blockers and exit rate of the last ion from the multi-ion pore of a K+ channel. *Science.* 271:653–656. http://dx.doi.org/10.1126/science.271.5249.653

Bezanilla, F. 2000. The voltage sensor in voltage-dependent ion channels. *Physiol. Rev.* 80:555–592.

Bezanilla, F., R.E. Taylor, and J.M. Fernández. 1982. Distribution and kinetics of membrane dielectric polarization. 1. Long-term inactivation of gating currents. *J. Gen. Physiol.* 79:21–40. http://dx.doi.org/10.1085/jgp.79.1.21

Bezanilla, F., E. Perozo, D.M. Papazian, and E. Stefani. 1991. Molecular basis of gating charge immobilization in Shaker potassium channels. *Science.* 254:679–683. http://dx.doi.org/10.1126/science.1948047

Bezanilla, F., E. Perozo, and E. Stefani. 1994. Gating of Shaker K+ channels: II. The components of gating currents and a model of channel activation. *Biophys. J.* 66:1011–1021. http://dx.doi.org/10.1016/S0006-3495(94)80882-3

Brew, H.M., J.X. Gittelman, R.S. Silverstein, T.D. Hanks, V.P. Demas, L.C. Robinson, C.A. Robbins, J. McKee-Johnson, S.Y. Chiu, A. Messing, and B.L. Tempel. 2007. Seizures and reduced life span in mice lacking the potassium channel subunit Kv1.2, but hypoexcitability and enlarged Kv1 currents in auditory neurons. *J. Neurophysiol.* 98:1501–1525. http://dx.doi.org/10.1152/jn.00640.2006

Bruening-Wright, A., and H.P. Larsson. 2007. Slow conformational changes of the voltage sensor during the mode shift in hyperpolarization-activated cyclic-nucleotide-gated channels. *J. Neurosci.* 27:270–278. http://dx.doi.org/10.1523/JNEUROSCI.3801-06.2007

Cha, A., and F. Bezanilla. 1997. Characterizing voltage-dependent conformational changes in the Shaker K+ channel with fluorescence. *Neuron.* 19:1127–1140. http://dx.doi.org/10.1016/S0896-6273(00)80403-1

Cuello, L.G., V. Jogini, D.M. Cortes, and E. Perozo. 2010. Structural mechanism of C-type inactivation in K(+) channels. *Nature.* 466:203–208. http://dx.doi.org/10.1038/nature09153

del Camino, D., and G. Yellen. 2001. Tight steric closure at the intracellular activation gate of a voltage-gated K(+) channel. *Neuron.* 32:649–656. http://dx.doi.org/10.1016/S0896-6273(01)00487-1

Dodson, P.D., B. Billups, Z. Rusznák, G. Szûcs, M.C. Barker, and I.D. Forsythe. 2003. Presynaptic rat Kv1.2 channels suppress synaptic terminal hyperexcitability following action potential invasion. *J. Physiol.* 550:27–33. http://dx.doi.org/10.1113/jphysiol.2003.046250

Douglas, C.L., V. Vyazovskiy, T. Southard, S.Y. Chiu, A. Messing, G. Tononi, and C. Cirelli. 2007. Sleep in Kcna2 knockout mice. *BMC Biol.* 5:42. http://dx.doi.org/10.1186/1741-7007-5-42

Doyle, D.A., J. Morais Cabral, R.A. Pfuetzner, A. Kuo, J.M. Gulbis, S.L. Cohen, B.T. Chait, and R. MacKinnon. 1998. The structure of the potassium channel: molecular basis of K+ conduction and selectivity. *Science.* 280:69–77. http://dx.doi.org/10.1126/science.280.5360.69

Glazebrook, P.A., A.N. Ramirez, J.H. Schild, C.C. Shieh, T. Doan, B.A. Wible, and D.L. Kunze. 2002. Potassium channels Kv1.1, Kv1.2 and Kv1.6 influence excitability of rat visceral sensory neurons. *J. Physiol.* 541:467–482. http://dx.doi.org/10.1113/jphysiol.2001.018333

Haddad, G.A., and R. Blunck. 2011. Mode shift of the voltage sensors in Shaker K^+ channels is caused by energetic coupling to the pore domain. *J. Gen. Physiol.* 137:455–472. http://dx.doi.org/10.1085/jgp.201010573

Hodgkin, A.L., and A.F. Huxley. 1952. A quantitative description of membrane current and its application to conduction and excitation in nerve. *J. Physiol.* 117:500–544.

Hoshi, T., W.N. Zagotta, and R.W. Aldrich. 1990. Biophysical and molecular mechanisms of Shaker potassium channel inactivation. *Science.* 250:533–538. http://dx.doi.org/10.1126/science.2122519

Kanevsky, M., and R.W. Aldrich. 1999. Determinants of voltage-dependent gating and open-state stability in the S5 segment of Shaker potassium channels. *J. Gen. Physiol.* 114:215–242. http://dx.doi.org/10.1085/jgp.114.2.215

Khavandgar, S., J.T. Walter, K. Sageser, and K. Khodakhah. 2005. Kv1 channels selectively prevent dendritic hyperexcitability in rat Purkinje cells. *J. Physiol.* 569:545–557. http://dx.doi.org/10.1113/jphysiol.2005.098053

Kuzmenkin, A., F. Bezanilla, and A.M. Correa. 2004. Gating of the bacterial sodium channel, NaChBac: voltage-dependent charge

movement and gating currents. *J. Gen. Physiol.* 124:349–356. http://dx.doi.org/10.1085/jgp.200409139

Labro, A.J., A.L. Raes, and D.J. Snyders. 2005. Coupling of voltage sensing to channel opening reflects intrasubunit interactions in Kv channels. *J. Gen. Physiol.* 125:71–80. http://dx.doi.org/10.1085/jgp.200409194

Lacroix, J.J., A.J. Labro, and F. Bezanilla. 2011. Properties of deactivation gating currents in Shaker channels. *Biophys. J.* 100:L28–L30. http://dx.doi.org/10.1016/j.bpj.2011.01.043

Liu, Y., M.E. Jurman, and G. Yellen. 1996. Dynamic rearrangement of the outer mouth of a K+ channel during gating. *Neuron.* 16:859–867. http://dx.doi.org/10.1016/S0896-6273(00)80106-3

Liu, Y., M. Holmgren, M.E. Jurman, and G. Yellen. 1997. Gated access to the pore of a voltage-dependent K+ channel. *Neuron.* 19:175–184. http://dx.doi.org/10.1016/S0896-6273(00)80357-8

Long, S.B., E.B. Campbell, and R. Mackinnon. 2005. Crystal structure of a mammalian voltage-dependent Shaker family K+ channel. *Science.* 309:897–903. http://dx.doi.org/10.1126/science.1116269

Loots, E., and E.Y. Isacoff. 1998. Protein rearrangements underlying slow inactivation of the *Shaker* K^+ channel. *J. Gen. Physiol.* 112:377–389. http://dx.doi.org/10.1085/jgp.112.4.377

MacKinnon, R. 1991. Determination of the subunit stoichiometry of a voltage-activated potassium channel. *Nature.* 350:232–235. http://dx.doi.org/10.1038/350232a0

Männikkö, R., S. Pandey, H.P. Larsson, and F. Elinder. 2005. Hysteresis in the voltage dependence of HCN channels: conversion between two modes affects pacemaker properties. *J. Gen. Physiol.* 125:305–326. http://dx.doi.org/10.1085/jgp.200409130

Murata, Y., H. Iwasaki, M. Sasaki, K. Inaba, and Y. Okamura. 2005. Phosphoinositide phosphatase activity coupled to an intrinsic voltage sensor. *Nature.* 435:1239–1243. http://dx.doi.org/10.1038/nature03650

Piper, D.R., A. Varghese, M.C. Sanguinetti, and M. Tristani-Firouzi. 2003. Gating currents associated with intramembrane charge displacement in HERG potassium channels. *Proc. Natl. Acad. Sci. USA.* 100:10534–10539. http://dx.doi.org/10.1073/pnas.1832721100

Ramaswami, M., M. Gautam, A. Kamb, B. Rudy, M.A. Tanouye, and M.K. Mathew. 1990. Human potassium channel genes: Molecular cloning and functional expression. *Mol. Cell. Neurosci.* 1:214–223. http://dx.doi.org/10.1016/1044-7431(90)90004-N

Rich, T.C., and D.J. Snyders. 1998. Evidence for multiple open and inactivated states of the hKv1.5 delayed rectifier. *Biophys. J.* 75:183–195. http://dx.doi.org/10.1016/S0006-3495(98)77505-8

Schoppa, N.E., and F.J. Sigworth. 1998. Activation of *Shaker* potassium channels. III. An activation gating model for wild-type and V2 mutant channels. *J. Gen. Physiol.* 111:313–342. http://dx.doi.org/10.1085/jgp.111.2.313

Shen, W., S. Hernandez-Lopez, T. Tkatch, J.E. Held, and D.J. Surmeier. 2004. Kv1.2-containing K+ channels regulate subthreshold excitability of striatal medium spiny neurons. *J. Neurophysiol.* 91:1337–1349. http://dx.doi.org/10.1152/jn.00414.2003

Shirokov, R., R. Levis, N. Shirokova, and E. Ríos. 1992. Two classes of gating current from L-type Ca channels in guinea pig ventricular myocytes. *J. Gen. Physiol.* 99:863–895. http://dx.doi.org/10.1085/jgp.99.6.863

Shu, Y., Y. Yu, J. Yang, and D.A. McCormick. 2007. Selective control of cortical axonal spikes by a slowly inactivating K+ current. *Proc. Natl. Acad. Sci. USA.* 104:11453–11458. http://dx.doi.org/10.1073/pnas.0702041104

Starace, D.M., and F. Bezanilla. 2001. Histidine scanning mutagenesis of basic residues of the S4 segment of the *Shaker* K^+ channel. *J. Gen. Physiol.* 117:469–490. http://dx.doi.org/10.1085/jgp.117.5.469

Starkus, J.G., L. Kuschel, M.D. Rayner, and S.H. Heinemann. 1997. Ion conduction through C-type inactivated *Shaker* channels. *J. Gen. Physiol.* 110:539–550. http://dx.doi.org/10.1085/jgp.110.5.539

Stefani, E., L. Toro, E. Perozo, and F. Bezanilla. 1994. Gating of Shaker K+ channels: I. Ionic and gating currents. *Biophys. J.* 66:996–1010. http://dx.doi.org/10.1016/S0006-3495(94)80881-1

Stühmer, W., J.P. Ruppersberg, K.H. Schröter, B. Sakmann, M. Stocker, K.P. Giese, A. Perschke, A. Baumann, and O. Pongs. 1989. Molecular basis of functional diversity of voltage-gated potassium channels in mammalian brain. *EMBO J.* 8:3235–3244.

Villalba-Galea, C.A., W. Sandtner, D.M. Starace, and F. Bezanilla. 2008. S4-based voltage sensors have three major conformations. *Proc. Natl. Acad. Sci. USA.* 105:17600–17607. http://dx.doi.org/10.1073/pnas.0807387105

Villalba-Galea, C.A., F. Miceli, M. Taglialatela, and F. Bezanilla. 2009. Coupling between the voltage-sensing and phosphatase domains of Ci-VSP. *J. Gen. Physiol.* 134:5–14. http://dx.doi.org/10.1085/jgp.200910215

Xiao, Y.F., N. Chandler, H. Dobrzynski, E.S. Richardson, E.M. Tenbroek, J.J. Wilhelm, V. Sharma, A. Varghese, M.R. Boyett, P.A. Iaizzo, and D.C. Sigg. 2010. Hysteresis in human HCN4 channels: a crucial feature potentially affecting sinoatrial node pacemaking. *Sheng Li Xue Bao.* 62:1–13.

Xie, G., J. Harrison, S.J. Clapcote, Y. Huang, J.Y. Zhang, L.Y. Wang, and J.C. Roder. 2010. A new Kv1.2 channelopathy underlying cerebellar ataxia. *J. Biol. Chem.* 285:32160–32173. http://dx.doi.org/10.1074/jbc.M110.153676

Yang, Y., Y. Yan, and F.J. Sigworth. 1997. How does the W434F mutation block current in *Shaker* potassium channels? *J. Gen. Physiol.* 109:779–789. http://dx.doi.org/10.1085/jgp.109.6.779

Yellen, G., M.E. Jurman, T. Abramson, and R. MacKinnon. 1991. Mutations affecting internal TEA blockade identify the probable pore-forming region of a K+ channel. *Science.* 251:939–942. http://dx.doi.org/10.1126/science.2000494

Zagotta, W.N., T. Hoshi, J. Dittman, and R.W. Aldrich. 1994. Shaker potassium channel gating. II: Transitions in the activation pathway. *J. Gen. Physiol.* 103:279–319. http://dx.doi.org/10.1085/jgp.103.2.279